Local distortions in $La_{0.7}Ca_{0.3}Mn_{1-b}A_bO_3$ (A=Ti and Ga) colossal magnetoresistance samples: Correlations with magnetization and evidence for cluster formation

D. Cao, F. Bridges, and M. Anderson
Department of Physics, University of California, Santa Cruz, California 95064

A. P. Ramirez and M. Olapinski
Bell Laboratories, Lucent Technologies, 600 Mountain Avenue, Murray Hill, New Jersey 07974-0636

M. A. Subramanian
Du Pont, Central Research & Development, Experimental Station, P.O. Box 80328, Wilmington, Delaware 19880-328

C. H. Booth and G. H. Kwei
Los Alamos National Laboratory, Los Alamos, New Mexico 87545
(Received 15 May 2001; published 17 October 2001)

X-ray absorption fine structure (XAFS) measurements as a function of temperature have been carried out at the Mn K edge for $La_{0.7}Ca_{0.3}Mn_{1-x}Ti_xO_3$ and $La_{0.7}Ca_{0.3}Mn_{1-y}Ga_yO_3$ (x and $y=0.01$ to 0.10) and correlated with transport and magnetization measurements. Most samples exhibit colossal magnetoresistance (CMR) at low temperature. The magnetization data show a concentration dependence: the ferromagnetic phase transition broadens as x or y increases, and both the transition temperature T_c and the saturated magnetization decrease with increasing dopant concentration. The transport measurements show that the resistivity increases as x or y increases, and that the resistivity peak, which we associated with the metal-to-insulator (MI) transition temperature T_{MI}, moves rapidly to lower temperatures with x or y. In contrast to the $La_{1-a}Ca_aMnO_3$ materials, for which the resistivity peak normally occurs very close to T_c, T_{MI} is usually far below T_c for these cosubstituted materials. The increase in resistivity well below T_c strongly suggests the formation of clusters. We also find that T_{MI} has a much smaller magnetic field dependence than that for $La_{1-a}Ca_aMnO_3$ CMR materials. The XAFS data show that a non-Debye broadening, associated with polaron formation, also develops as T approaches T_c, as observed for other CMR samples, but the magnitude of this extra broadening, $\Delta\sigma^2$, decreases with x or y, with a larger effect for Ti than for Ga. We find that for a given type of dopant, the resistivity peak occurs when σ^2 is decreased to a specific value that is essentially independent of concentration and that this corresponds to nearly the same value of the sample magnetization. These results indicate that the addition of either Ga or Ti distorts the local Mn-O environment which likely promotes cluster formation. Measurements of the absorption edge shift as a function of x for these materials do not quite follow the calculated edge positions based on concentrations, possibly suggesting small variations in O stoichiometry.

DOI: 10.1103/PhysRevB.64.184409 PACS number(s): 75.30.Vn, 61.10.Ht, 71.38.−k

I. INTRODUCTION

The $La_{1-a}Ca_aMnO_3$ (LCMO) series of Colossal Magnetoresistance (CMR) materials have been studied extensively, in part because of their novel transport properties. The basic mechanism which couples the spin and charge in these materials is generally assumed to be the double exchange (DE) model.[1–3] In this model, an electron will hop more easily from one Mn site to another if both Mn site moments are aligned. As a result of the DE mechanism, the system will become ferromagnetic (FM) below the transition temperature, T_c. However, recent research has shown that the DE model alone, cannot explain the large magnetoresistance (MR) of CMR materials.[4,5] It is generally accepted that a strong lattice distortion is present above T_c that greatly decreases the electron hopping rate. These distortions are often described in terms of small lattice polarons which form above T_c.[4–8]

Recent experiments, using x-ray absorption fine structure (XAFS) and neutron pair distribution function (PDF) techniques, have been carried out to study the local structure of LCMO CMR materials; a polaronlike local distortion has indeed been found[9–15] and its temperature dependence has been investigated.

A starting point for many discussions of these CMR systems is to assume there is a mixture of Mn^{+3} and Mn^{+4} sites (although there is considerable covalency) with the fraction of Mn^{+4} determined by the Ca dopant level (for $a=0.3$, 30% of the Mn sites would be Mn^{+4}). In this experiment we investigate the effect of replacing a small fraction of the Mn by either +3 or +4 ions, to better understand the role of Mn and its local environment in determining other physical properties. If we use Ti or Ga to replace some of the Mn in these materials, then Ti^{4+} should replace Mn^{4+}, and Ga^{3+} should replace Mn^{3+}. The ionic radius[16] of Ga^{3+} (0.620 Å) is comparable to, but slightly smaller than that for Mn^{3+} (0.645 Å), while the radius for Ti^{4+} (0.605 Å) is larger than that Mn^{4+} (0.530 Å) although comparable to Mn^{3+}. Thus Ti substitution should produce larger strains. In addition, there are other aspects to these substitutions that must be considered; removing an Mn^{3+} site removes four magnetic electrons while removing Mn^{4+}, removes only three. In

addition, although the valence on a particular Mn atom normally fluctuate as electrons move through the material, both Ga^{3+} and Ti^{4+} pin the valence of a particular site at a fixed value.

Neutron diffraction studies of a number of these samples indicate that the orthorhombic structures remain essentially the same as the undoped $La_{0.7}Ca_{0.3}MnO_3$ compound. However, transport and magnetization measurements show that both the resistivity and magnetization of the material change significantly with small amounts of Ti or Ga in the sample; the resistivity increases, particularly at low T, and the saturation magnetization decreases more than expected from the decrease in the number of Mn atoms. The local structure, obtained via EXAFS, also changes; the temperature dependence of the broadening parameter (Debye-Waller parameter) σ^2 for the Mn-O bond becomes weaker as the concentration of Ti or Ga dopant increases.

Correlations between local structure, resistivity and magnetization are again found in these samples and will be discussed and compared with earlier results. Surprisingly the correlations between local structure and magnetization occur over a wide range of temperatures (20 K to T_c) and hence over a wide range of magnetization. Only the broadened tail of the transition (nonzero magnetization above T_c) does not fit well. However, the resistivity peak at T_{MI} occurs in the middle of this range, far below T_c, and the resistivity is double-valued when plotted as a function of either magnetization or σ^2. We propose that the low value of T_{MI} is the result of the formation of magnetic conducting clusters within a highly resistive region, and that the resistivity does not decrease until the regions between the magnetic clusters become thin.

X-ray absorption near edge structure (XANES) measurements at the Mn K edge were also carried out to probe the valence changes induced by the substitution of Ti and Ga for Mn. The edge shifts roughly follow the predicted positions based on composition, but in some cases deviation in edge positions suggests a small variation in the O stoichiometry.

In this paper, the samples and experimental details are discussed in Sec. II, and the magnetization and transport results are reported in Sec. III. The Mn K-edge XANES studies are presented in Sec. VI and the XAFS data and data analysis given in Sec. V. Finally, the discussion and the conclusions are discussed in Secs. VI and VII, respectively.

II. EXPERIMENTAL DETAILS

A. Samples

The samples used in these experiments are $La_{0.7}Ca_{0.3}Mn_{1-x}Ti_xO_3$ and $La_{0.7}Ca_{0.3}Mn_{1-y}Ga_yO_3$, with $x,y=0.01$, 0.02, 0.04, 0.06, 0.08, or 0.10. The compounds were prepared by the conventional powder sintering technique using starting materials with a purity of 99.9% or higher. La_2O_3 was heated at 1000 °C before use. The materials were weighed according to the stoichiometric ratios and mixed thoroughly in an agate mortar. The mixed powder was calcined at 900–1000 °C for 8 h. The calcined powder was reground and pressed into disks of 12.7 mm diameter/1–2 mm thickness. The disks were sintered in air at 1000–1100 °C for 20 h. The ramping rate was 200 °C/h and the cooling rate was 150 °C/h. Thermogravimetric analysis in the temperature range 300–1000 K did not show any evidence for oxygen intake or oxygen removal from the samples. Wet chemical analysis of representative samples using iodometric titration indicated no observable deviation in oxygen stoichiometry from that calculated using the composition. This sets an upper limit to the Mn valence uncertainty within 0.05 valence units.

B. Experimental procedures

All the samples are magnetic and most exhibit CMR. The resistivity measurements were carried out using a four-wire (van der Pauw) geometry and the magnetization measurements were done on pressed pellets using a SQUID magnetometer.

In our EXAFS experiments, we reground the powdered sample and used a 400-mesh sieve to obtain a fine powder, which was then brushed onto Scotch tape. We used two double layers of the tape to obtain $\Delta\mu_{\mathrm{Mn}}\cdot t\sim 0.5$ for each sample in these experiments ($\Delta\mu_{\mathrm{Mn}}$ is the x-ray absorption coefficient for the Mn K edge and t is the thickness of the powder sample). The XAFS experiments were done on beamline 4-3 at Stanford Synchrotron Radiation Laboratory (SSRL) using Si $\langle 111\rangle$ monochromator crystals. All data were collected in the transmission mode. We used a powdered Mn metal sample as an energy reference in order to study the near-edge structure. Data analysis was done using the programs REDUCE and FITX (Refs. 17,18) with theoretical functions generated using FEFF6.[19]

C. XAFS technique

When a photoelectron is ejected from an atom by the incoming x ray, the outgoing electron wave will interfere with the waves backscattered by other atoms and thereby change the absorption coefficient μ.[20,21] As the incident x-ray energy changes, the interference varies from constructive to destructive, producing oscillations in μ. The absorption coefficient can be written as $\mu=\mu_0(1+\chi)$, where μ_0 is the background (embedded atom) function[22] and χ is the XAFS function. $k\chi$ is theoretically given as

$$k\chi(k)=\mathrm{Im}\sum_i A_i\int_0^\infty F_i(k,r)\frac{g_i(r_{0i},r)e^{i[2kr+2\delta_c(k)+\delta_i(k)]}}{r^2}dr, \tag{1}$$

where the amplitude factor A_i is given by

$$A_i=N_iS_0^2, \tag{2}$$

and the photoelectron wave vector k is given by $k=\sqrt{2m_e(E-E_0)/\hbar^2}$, E_0 is the binding energy for a certain shell of electrons. $g_i(r_{0i},r)$ is the pair distribution function (we use a Gaussian function here) for the atoms at a distance r_{0i}, and $\delta_c(k)$ and $\delta_i(k)$ are the phase shifts of the central and backscattered photoelectron waves respectively. $F_i(k,r)$ is the backscattering amplitude of the photoelectron wave

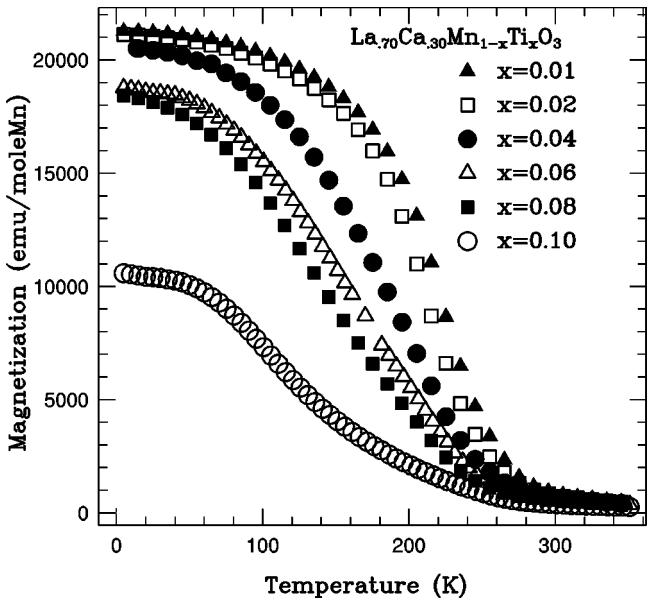

FIG. 1. Magnetization vs temperature for the Ti doped samples. Magnetization measurements were done using a SQUID magnetometer. The saturated magnetization drops as the Ti concentration x increases, while the Curie temperature changes slowly with x.

from shell i which includes a mean-free path term, N_i is the number of atoms in shell i, and S_0^2 is a correction for multielectron effects.

A Fourier transform of $k\chi(k)$ yields peaks in r space which correspond to the different atomic shells—but shifted in position as a result of the k dependence of the phase shifts $\delta_c(k)$, $\delta_i(k)$. Fits to the data can be carried out to determine the position, amplitude (coordination number) and broadening parameter σ for several different shells of neighbors.

III. MAGNETIZATION AND RESISTIVITY MEASUREMENTS

In Fig. 1 we present the magnetization vs temperature data for the Ti doped samples. The plot shows that the saturation magnetization M_0 decreases as x increases; for low concentrations the decrease is comparable to the value expected when nonmagnetic Ti replaces Mn^{+4}. However, by 8% Ti the suppression is about twice that calculated, and for $x=0.10$ sample, M_0 is almost 50% smaller than that for the 0.01 sample. Thus as x increases, the ferromagnetic fraction in the sample becomes smaller, and shrinks faster than the decrease in the number of Mn atoms. This may be due to the formation of nonferromagnetic (possibly antiferromagnetic) areas around Ti ions. The FM phase transition of these samples broadens considerably with x, yet there are only small changes in the Curie temperature T_c (defined by the intersection of a straight line through the steepest slope, with the x axis). T_c varies from ~ 270 K for the $x=0.01$ sample to ~ 220 K for the $x=0.10$ sample, a range of ~ 50 K.

Figure 2 shows the resistivity vs temperature data for the Ti doped samples on a log-linear plot, at zero field (top panel) and 6 T (lower panel). At low temperatures, the resistivity increases rapidly with x, although the Ti concentration

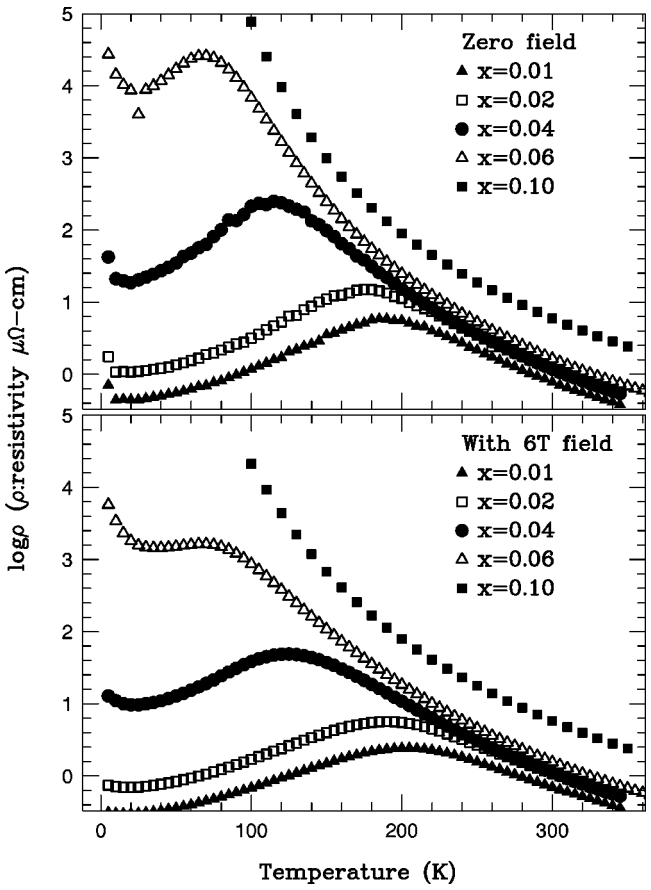

FIG. 2. $\log \rho$ vs temperature for the Ti doped samples. The upper window shows the data at zero field, while the lower window shows the data for a 6 T field. The resistivity at low-temperature increases dramatically with x, while at high temperatures it only changes slowly with x. All resistivity curves are parallel at high temperature, which indicates that each sample has a similar polaron activation energy at high temperature.

is quite small. At high temperature, the change of resistivity with x is much smaller. Note however, that above T_c the curves are all parallel. This means that the activation energy for polarons[23] at high temperature is nearly independent of x. Consequently, the increased resistivity at high T (room temperature) must indicate a decrease in the carrier density with increasing Ti doping, i.e., some carriers become localized, probably at or near the Ti.

The resistivity peak in Fig. 2 is shifted to lower temperature as x increases, and in each case T_{MI} is well below T_c (see Table I). In contrast, the resistivity peak is very close to T_c for $La_{0.7}Ca_{0.3}MnO_3$. This suggests that these two types of transitions may be independent with no obvious relationship between them for these co-doped samples. In particular, the position of T_{MI} appears to be a competition between the conducting and nonconducting regions and their connectivity. For the $x=0.10$ sample the resistivity increases rapidly at low T and there is no metal-to-insulator phase transition down to 100 K. Lower temperature data for this sample are not available because of the very large resistivity below 100 K.

Comparing the magnetization and the resistivity data for

TABLE I. A comparison of the Curie temperature T_c and the resistivity peak temperature T_{MI} (the metal-to-insulator phase transition) for the Ti and Ga doped samples.

Material	T_c (K)	T_{MI} (K)
$La_{0.7}Ca_{0.3}Mn_{0.99}Ti_{0.01}O_3$	271(5)	185(5)
$La_{0.7}Ca_{0.3}Mn_{0.98}Ti_{0.02}O_3$	262(5)	175(5)
$La_{0.7}Ca_{0.3}Mn_{0.96}Ti_{0.04}O_3$	262(5)	115(5)
$La_{0.7}Ca_{0.3}Mn_{0.94}Ti_{0.06}O_3$	261(5)	70(5)
$La_{0.7}Ca_{0.3}Mn_{0.92}Ti_{0.08}O_3$	243(5)	N/A
$La_{0.7}Ca_{0.3}Mn_{0.90}Ti_{0.10}O_3$	217(5)	N/A
Material	T_c	T_{MI}
$La_{0.7}Ca_{0.3}Mn_{0.99}Ga_{0.01}O_3$	289(5)	185(5)
$La_{0.7}Ca_{0.3}Mn_{0.98}Ga_{0.02}O_3$	270(5)	200(5)
$La_{0.7}Ca_{0.3}Mn_{0.96}Ga_{0.04}O_3$	261(5)	155(5)
$La_{0.7}Ca_{0.3}Mn_{0.94}Ga_{0.06}O_3$	238(5)	N/A
$La_{0.7}Ca_{0.3}Mn_{0.92}Ga_{0.08}O_3$	220(5)	N/A
$La_{0.7}Ca_{0.3}Mn_{0.90}Ga_{0.10}O_3$	197(5)	N/A

the Ti doped samples, we find that the resistivity continues to increase well below T_c even though the lattice on average has become less distorted (see Sec. V). The difference between T_c and T_{MI} can approach 200 K as shown in Table I.

Another surprising result for Ti (and also Ga) doping is that T_{MI} does not shift much in a magnetic field, in contrast to other CMR materials we have studied previously.[9,10] Typically, the resistivity peak shifts to higher temperature when applying a magnetic field, and it is generally a significant shift. For example, T_{MI} shifts about 40–50 K for the 30% Ca doped LCMO thin film samples.[12] However, for this set of codoped samples, T_{MI} only changes about 20 K for the 0.01 Ti doped sample and has almost no shift for the 0.06 Ti doped sample.

The magnetoresistivity data for the Ti doped samples are shown in Fig. 3. In this plot MR% is defined as

$$\mathrm{MR\%} = 100[\rho(0) - \rho(H)]/\rho(H), \tag{3}$$

where $\rho(H)$ and $\rho(0)$ represent the resistivity of the sample with and without a magnetic field, respectively. The magnetoresistivity peak occurs at almost the same temperature as the resistivity peak. Also as x increases, the magnitude of the MR peak increases, although we cannot verify this result for the 0.1 sample.

The magnetization data for the Ga doped samples are shown in Fig. 4 and have a very similar behavior to those for the Ti doped samples. The saturation magnetization M_0 also decreases with y but this decrease is smaller than for Ti, and closer to the expected decrease if nonmagnetic Ga^{+3} replaces Mn^{+3}, the exception being the 10% Ga sample. This suggests that the nonferromagnetic regions induced around the Ga ions are smaller than those for the Ti doped samples. T_c decreases from ~ 280 K at $y=0.02$ to 200 K at $y=0.1$, and the ferromagnetic transition becomes somewhat broader with y. Note that the $y=0.01$ Ga doped sample has a different behavior compared to the other samples and is likely inhomogeneous.

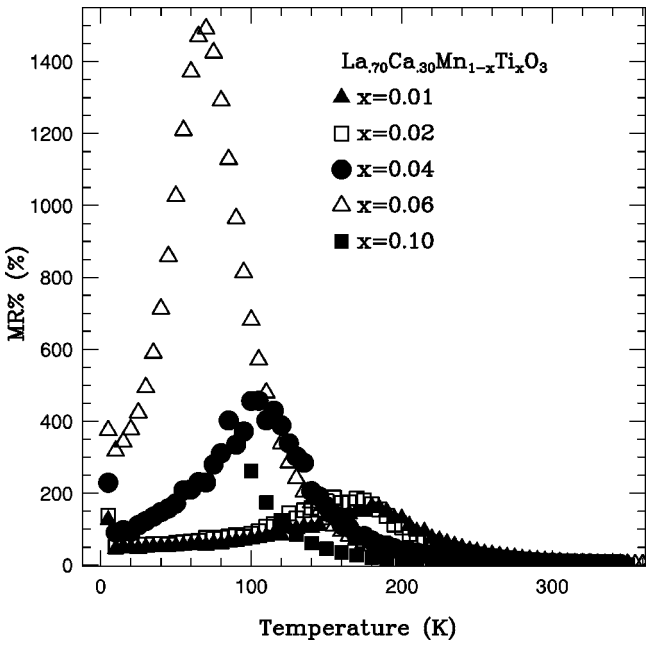

FIG. 3. A plot of magnetoresistivity (MR%) vs temperature for Ti doped CMR samples. MR% is defined in Eq. (3). $\rho(H)$ is measured in a 6 T magnetic field.

The resistivity data (on a log-linear plot) are shown in Fig. 5 for four of the Ga doped samples, with $B=0$ and 6 T. The resistivity data follow the same trends as for the Ti doped samples, except again for the inhomogeneous $y=0.01$ sample. In particular, there is very little shift of the resistivity peak temperature with applied magnetic field and

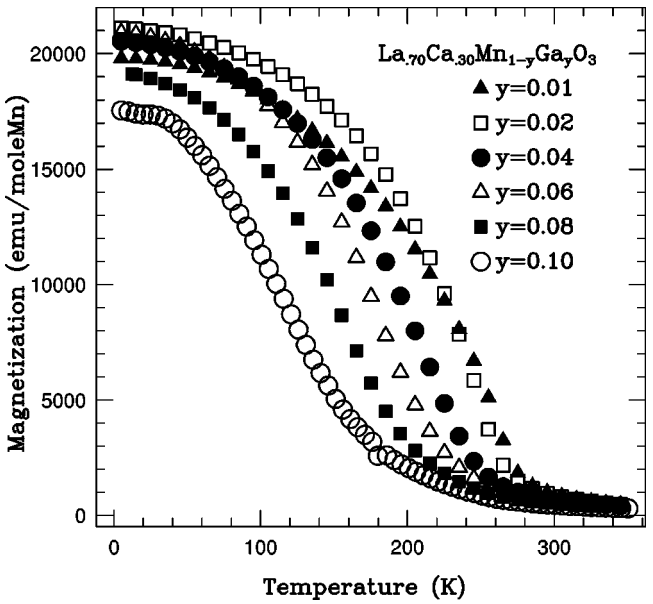

FIG. 4. Magnetization data for the $La_{0.70}Ca_{0.30}Mn_{1-y}Ga_yO_3$ samples. The $y=0.01$ sample does not follow the trend of the other samples and appears to be inhomogeneous. The saturated magnetization follows the same trend as for the Ti doped samples with a smaller concentration effect. The change in Curie temperature with Ga concentration is larger than that for the Ti doped samples.

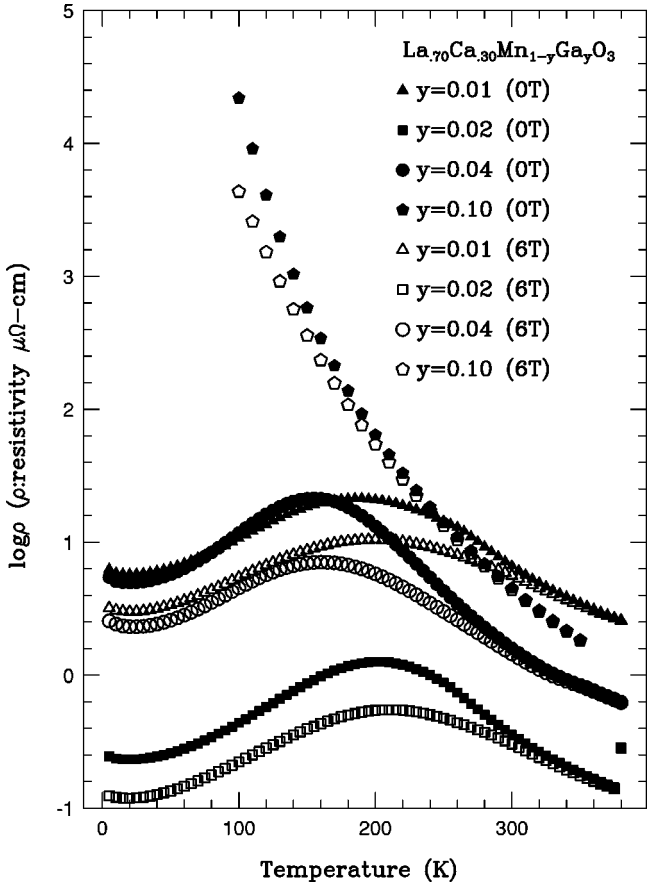

FIG. 5. Resistivity data for Ga doped $La_{0.7}Ca_{0.3}MnO_3$ samples in zero and a 6 T field. Only four samples were measured; the amount of material available for the $y=0.06$ and 0.08 powdered samples was too small for resistivity measurements.

the slope at high temperature is nearly the same for all except the $y=0.10$ sample, which does not have a resistivity peak down to 100 K.

Figure 6 shows the magnetoresistivity data for four Ga doped samples. The MR peak moves to lower temperature and again the magnitude of the peak increases with y. Compared with the Ti doped samples, the magnetoresistivity for the Ga doped samples is smaller. The inhomogeneity of the $y=0.01$ sample is shown clearly in this figure, with a peak at 150 K and a shoulder at ~ 267 K. This suggests a mixture of very low doped regions ($T_c \sim 270$ K) with regions having a higher concentration of Ga ($y \sim 0.03$; $T_c \sim 150$ K).

IV. MN *K*-EDGE XANES

In recent studies,[10,14,24–27] the energy of the average Mn-*K* edge shifts nearly linearly with the Mn valence of the LCMO samples as determined by the composition. When the average valence of Mn in the sample changes from $+3$ ($LaMnO_3$) to $+4$ ($CaMnO_3$) the position of the main edge shifts about 3 eV (using the peak in the first derivative, the net shift is about 4.2 eV (Refs. 10,14) but the position of the inflection point moves on the edge relative to the half height). In this section we report the average edge shifts for the Ti^{+4} and Ga^{+3} codoped LCMO samples.

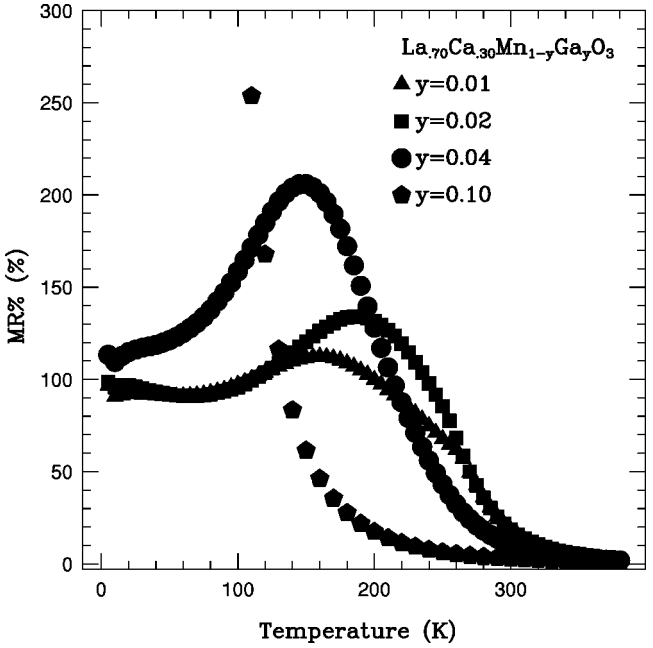

FIG. 6. A plot of MR% vs temperature for the Ga doped CMR samples. The data for the $y=0.01$ sample shows a double peak structure, which suggest that the sample is inhomogeneous.

Table II shows the concentration of Ti^{+4} and Ga^{+3} ions, the average Mn valence, and the predicted concentrations of Mn^{+3} and Mn^{+4}, assuming ionic behavior and perfect stoichiometry.

Transmission Mn *K*-edge XAFS data were collected simultaneously for both the manganite and Mn-metal reference samples. The upper panel of Fig. 7 shows the absorption coefficient μ as a function of energy for one of the samples. For both the XANES and EXAFS studies, a pre-edge absorp-

TABLE II. The average Mn valence and the relative fractions of Mn^{+4} and Mn^{+3} sites in both the Ti and Ga doped LCMO samples. Titration measurements yield a value for the Mn valence that is consistant with the stoichiometric value. However, the titration measurements are only sensitive to ± 0.05 Mn valence unit. This places an upper limit on the valence uncertainty.

Material	$[Ti^{+4}]$	Mn valence	$[Mn^{+4}]$	Mn^{+3}
$La_{0.7}Ca_{0.3}Mn_{0.99}Ti_{0.01}O_3$	0.01	3.293	0.29	0.7
$La_{0.7}Ca_{0.3}Mn_{0.98}Ti_{0.02}O_3$	0.02	3.286	0.28	0.7
$La_{0.7}Ca_{0.3}Mn_{0.96}Ti_{0.04}O_3$	0.04	3.271	0.26	0.7
$La_{0.7}Ca_{0.3}Mn_{0.94}Ti_{.06}O_3$	0.06	3.255	0.24	0.7
$La_{0.7}Ca_{0.3}Mn_{0.92}Ti_{0.08}O_3$	0.08	3.239	0.22	0.7
$La_{0.7}Ca_{0.3}Mn_{0.90}Ti_{0.10}O_3$	0.10	3.222	0.20	0.7
Material	$[Ga^{+3}]$	Mn valence	$[Mn^{+4}]$	Mn^{+3}
$La_{0.7}Ca_{0.3}Mn_{0.99}Ga_{0.01}O_3$	0.01	3.303	0.3	0.69
$La_{0.7}Ca_{0.3}Mn_{0.98}Ga_{0.02}O_3$	0.02	3.306	0.3	0.68
$La_{0.7}Ca_{0.3}Mn_{0.96}Ga_{0.04}O_3$	0.04	3.313	0.3	0.66
$La_{0.7}Ca_{0.3}Mn_{0.94}Ga_{0.06}O_3$	0.06	3.319	0.3	0.64
$La_{0.7}Ca_{0.3}Mn_{0.92}Ga_{0.08}O_3$	0.08	3.326	0.3	0.62
$La_{0.7}Ca_{0.3}Mn_{0.90}Ga_{0.10}O_3$	0.10	3.333	0.3	0.60

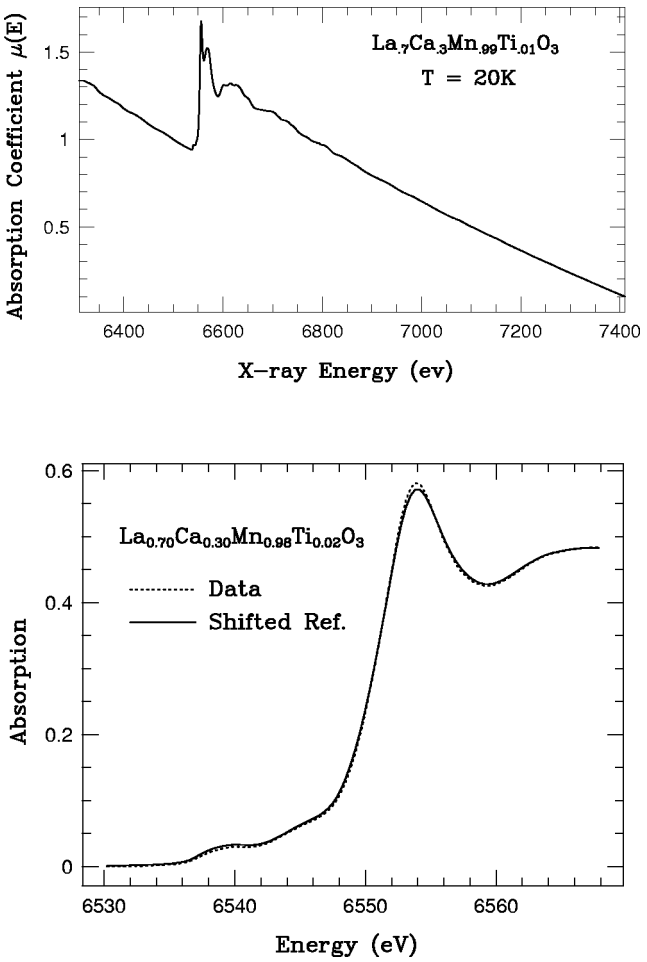

FIG. 7. Upper panel: The absorption data for Mn *K* edge. Bottom panel: A plot of the edge for $La_{0.70}Ca_{0.30}Mn_{0.98}Ti_{0.02}O_3$ and the fit of a reference trace ($La_{0.70}Ca_{0.30}MnO_3$) to it. (Pre-edge background has been removed.)

tion (absorption from other edges) must first be removed; this was accomplished via a background removal which uses the Victoreen formula. To find the relative edge shifts, it is important to first normalize the data well above the edge and ensure that the baseline below the edge is at zero.

Edge shifts for Ti and Ga samples were obtained as a function of concentration using the 320 K measurements. Data for each concentration were fit to the $La_{0.70}Ca_{0.30}MnO_3$ edge (which serves as a reference data trace), by shifting the edge position for $La_{0.70}Ca_{0.30}MnO_3$ until it overlaps the data trace. An example of such a fit is shown in Fig. 7. The shifts were generally averaged over three scans. For each concentration, the edge for the Mn metal reference sample was fit in a similar manner to the Mn metal reference edge collected with the $La_{0.70}Ca_{0.30}MnO_3$ sample, to correct for any drift in the x-ray energy calibration, and again averaged. The sample and Mn powder reference shifts were then combined together to get the net relative shift. Expected shifts were calculated assuming that the samples were stoichiometric and that one valence unit corresponds to an edge shift of 3 eV.

The experimental edge shifts are plotted in Fig. 8 for $La_{0.70}Ca_{0.30}Mn_{1-x}Ti_xO_3$; the data do not quite follow the expected shifts and the experimental shift does not change much between 1–8 % Ti. However, because the estimated error is ± 0.04 eV, the difference between experiment and these ideal calculations is not very significant except for $x = 0.1$. The 10% sample shows an unexpected positive shift of roughly 0.16 eV relative to the calculated value. Nearly identical results were also obtained using the 50 K data. One possible explanation for the discrepancies between the experimental results and the calculated values is that the oxygen concentration may vary from sample to sample (for example, a low O concentration for 1% and excess O for the 10% sample); however the variations are still within the upper limit for the uncertainty in the Mn valance obtained from titration; 0.05 valence units $= 0.15$ eV.

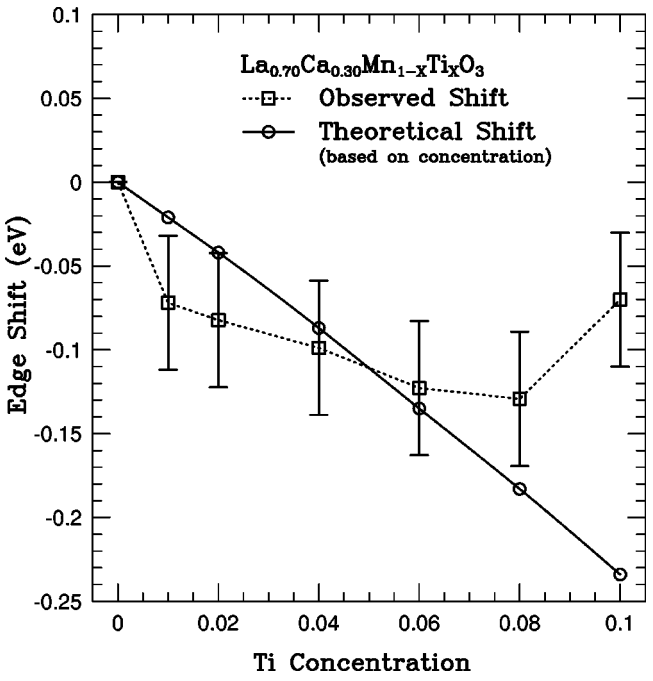

FIG. 8. The shift of the Mn *K* edge with Ti concentration for $La_{0.70}Ca_{0.30}Mn_{1-x}Ti_xO_3$. The relative errors are ± 0.04 eV.

The experimental edge shifts were also obtained for the Ga doped samples: $La_{0.70}Ca_{0.30}Mn_{1-y}Ga_yO_3$ with $y = 0$, 1, 2, 4, 6, 8, and 10 %. Edge data for a 20% Ga doped sample is shown in this figure, but there is no XAFS data for this sample since it is too disordered. The experimental shift follows the same upward trend as predicted theoretically but the shifts are larger than expected, as shown in Fig. 9. The large discrepancies for some samples and an overall positive shift of roughly 0.08 eV might again be attributed to a nonstoichiometric oxygen concentration in the samples, in this case an excess of O. The large shifts for the 1, 6, and 8 % samples are larger than the upper limit to the error in Mn valence, obtained from titration.

V. XAFS DATA REDUCTION AND ANALYSIS

To extract the XAFS oscillations above the edge, a five-knot cubic spline was used to determine the background function μ_0. χ(k) is then calculated from $\chi(k) = \mu/\mu_0 - 1$;

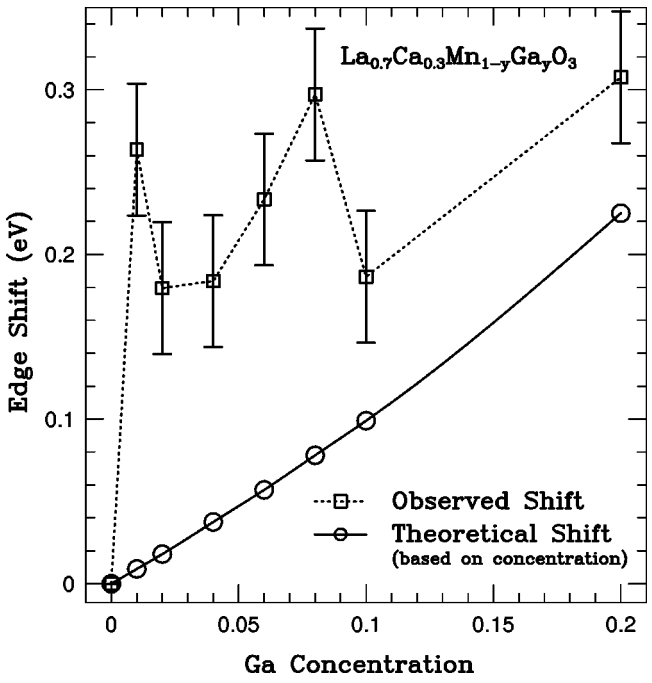

FIG. 9. The shift of the Mn *K* edge with Ga concentration for $La_{0.70}Ca_{0.30}Mn_{1-y}Ga_yO_3$. The relative errors are ± 0.04 eV.

an example is shown in Fig. 10.

The *r*-space data were obtained from the Fourier Transform (FT) of $k\chi(k)$; and fits of the data were carried out in *r* space. A brief discussion of these fits is provided later in this section; for additional details, please see Ref. 10.

Figure 11 shows the Mn *K*-edge Fourier transformed *r*-space data for three of the Ti doped samples ($x=0.01$, 0.06, 0.10, respectively); a temperature dependence is clearly present. In the *r*-space data, each peak corresponds to a certain atom shell with a well understood phase shift. We fit all peaks out to 3.8 Å using Gaussian pair distribution functions; in this case, Mn-O, Mn-La/Ca, and Mn-Mn (plus multiscattering peaks) pairs were used.

The width of the pair distribution function σ is a measure of the distribution of atom-pair separations. Here, we focus primarily on local distortions of the Mn-O bond, which corresponds to the first peak in the *r*-space data. A large sigma

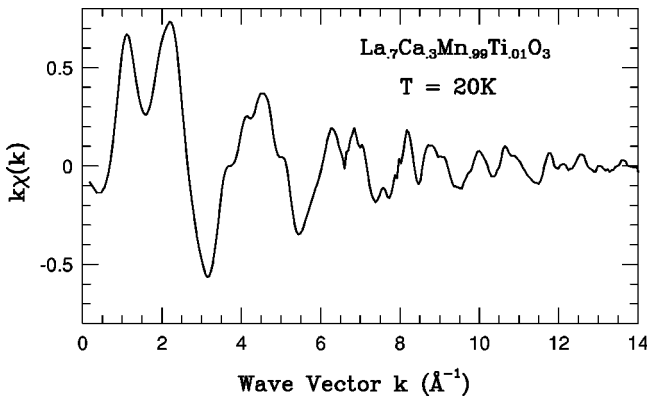

FIG. 10. The *k* space data for the $x=0.01$ Ti doped sample at 20 K, which shows the quality of the data.

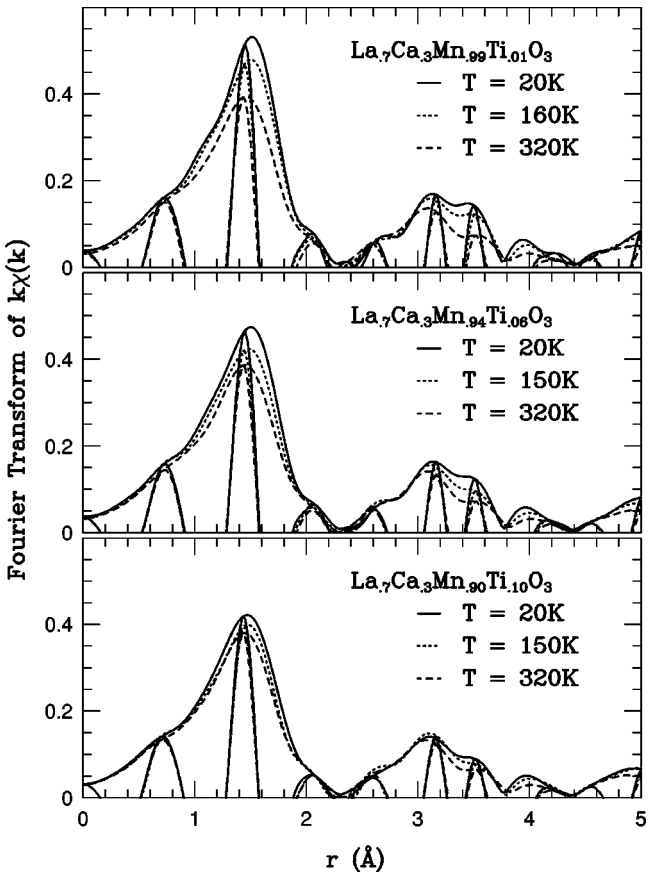

FIG. 11. A plot of the *r*-space data for three Ti doped $La_{0.70}Ca_{0.30}MnO_3$ samples ($x=0.01$, 0.06, and 0.10), at three temperatures. The FT range is 3.3–13.0 $Å^{-1}$, with 0.3 $Å^{-1}$ Gaussian broadening. The high frequency curve inside the envelope is the real part of the FT (FT_R). The envelop, is defined as $\sqrt{FT_R^2+FT_I^2}$ where FT_I is the imaginary part of the FT, and each peak of the envelope represents a certain atom shell around the center atom Mn.

indicates a large local distortion in the MnO_6 octahedra and leads to a small amplitude in the *r*-space peak.

Some initial results about the change of the Mn-O local distortion with *x* and temperature *T*, can be obtained from Fig. 11. The local distortion increases with *T* for all samples, but the relative change becomes smaller and a static disorder contribution at low temperature increases as *x* increases. However, at 300 K, the Mn-O peak amplitude changes only a few percent with *x*. This indicates that the local distortions, present at high temperature, are only partially removed at low temperature, for the higher Ti concentrations.

The *r*-space data for Ga doped samples are shown as a function of temperature in Fig. 12 for $y=0.02$, 0.06, 0.10. The data follow the same trend as for the Ti doped samples; the amplitude of the first peak still decreases with temperature for all the samples. However, the difference in this change between the lowest and highest concentration sample is smaller than that for the Ti doped samples. We use the $y=0.02$ sample for the low concentration sample instead of $y=0.01$ in Fig. 12, because the latter is inhomogeneous. (Note that the $x=0.01$ and 0.02 Ti doped samples have very similar behavior—only a small difference exists; we there-

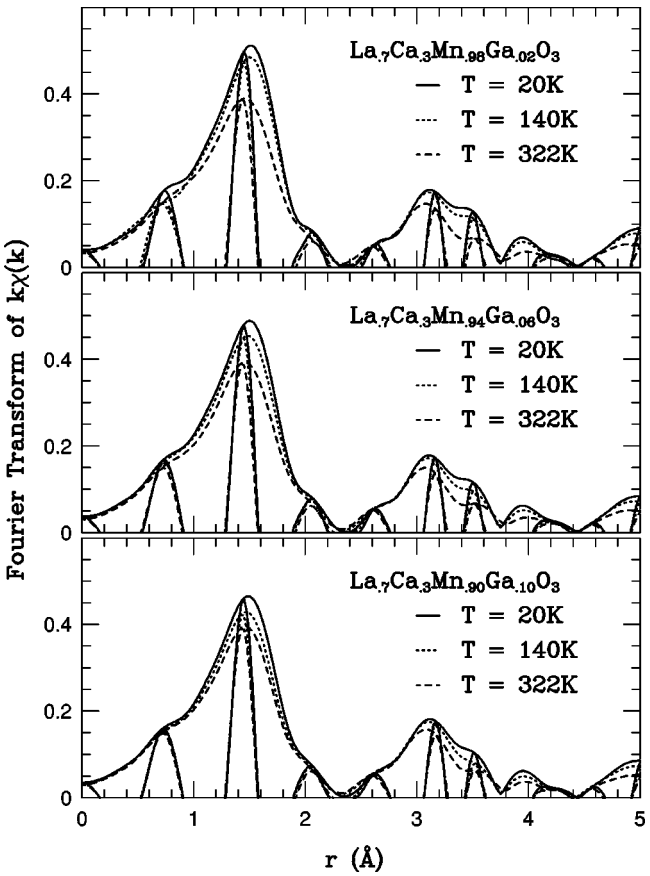

FIG. 12. A plot of the *r*-space data for three Ga doped $La_{0.70}Ca_{0.30}MnO_3$ samples ($y=0.02$, 0.06, 0.10 from top to bottom) at 20, 140, and 322 K. The FT range is the same as used for the Ti doped samples (3.3–13.0 $Å^{-1}$).

fore compare between the $y=0.02$ Ga and $x=0.01$ Ti *r*-space data sets.)

Our fits were carried out in *r*-space using theoretical functions obtained using the code FEFF6.[19] We use Gaussian pair distribution functions and extracted the width σ for the Mn-O peak. In these fits, S_0^2N for the Mn-O pair was fixed to be 4.3, as determined in previous studies of these materials;[10] here N is 6 (the number of nearest oxygen neighbors).

For the Mn-O bond, σ^2 has in general several contributions which add in quadrature:

$$\sigma^2=\sigma^2_{\text{static}}+\sigma^2_{\text{phonons}}+\sigma^2_{\text{other mechanisms}}. \tag{4}$$

Here σ^2_{static} comes from any static disorder that exists in the sample; it may arise from interstitials, vacancies, strain, etc; $\sigma^2_{\text{phonons}}$ is a measure of thermally generated vibrations; $\sigma^2_{\text{other mechanisms}}$ is a measure of local distortion coming from other mechanisms, in this case, a *T*-dependent polaronlike distortion. For additional discussion, see Ref. 12.

The change of σ^2 as a function of temperature is shown in Fig. 13 for the Ti doped samples. The solid line in the lower part of the figure is the thermal contribution to σ^2, which is defined as $\sigma^2_{\text{phonons}}$ above. This solid line is obtained from $CaMnO_3$ which has a very high Debye temperature, and shows how σ^2 would change with temperature without a

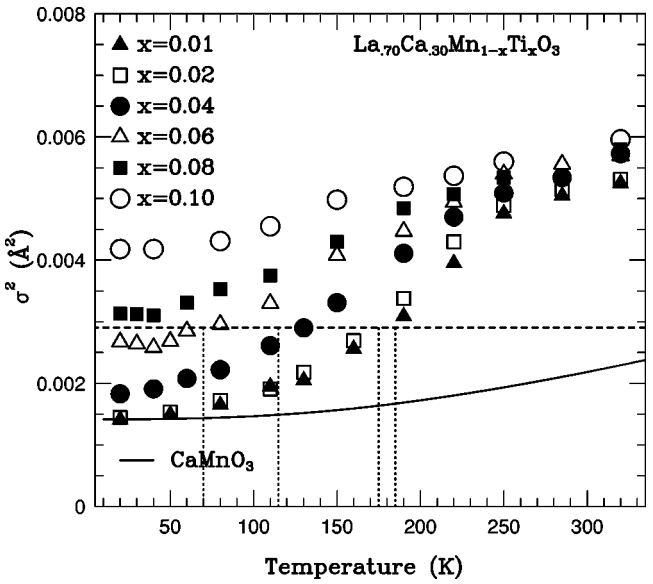

FIG. 13. A plot of σ^2 vs temperature for the Mn-O bond in the Ti doped samples. Relative error bars are approximately the same size as the symbols, and are not shown in this plot. The vertical dotted lines show the position of the peak in resistivity T_{MI} for $x=0.01$, 0.02, 0.04, and 0.06 Ti doped samples. The horizontal line passes through the values of σ^2 at T_{MI} for each sample. This determines σ_c.

polaron distortion in the sample. We refer to this dependence as ''Debye broadening.'' Figure 13 shows that every sample has a non-Debye broadening component, which is a steplike structure attributed to the formation of polarons near T_c. The break points in the curves for 1–8 % Ti vary from 200 to 250 K, and are very close to T_c for each case. Although the resistivity peaks occur at much lower temperatures (185 to 70 K) as the Ti concentration increases from 0.01 to 0.06 (Fig. 2), the local structure for each sample changes smoothly over this range of temperature. Thus, the data show that changes in local structure correlate well with the magnetization but not the resistivity. The small difference at 300 K (Fig. 13), ~ 0.0008 $Å^2$ from the 0.01 sample to the 0.10 sample, indicates that the static distortion in the sample also increases slightly with *x*. Another obvious result is that the change of local structure associated with polaron formation (essentially the step height change between 20 K and T_c in Fig. 13) decreases as *x* increases.

The vertical dotted lines in Fig. 13 represent the resistivity peak temperatures T_{MI}, for, from left to right, the 0.06 to 0.01 samples. The dashed horizontal line is determined by the point at which these vertical lines cross the corresponding σ^2 vs *T* plot. However, why T_{MI} occurs at the *same* value of σ^2 for each Ti concentration is not clear. This observation suggests that only when the local distortion in the sample has decreased to a certain critical value σ_c can the metal-to-insulator phase transition occur.

In Fig. 14, we plot σ^2 vs *T* for the Ga doped samples to compare with the data for the Ti doped samples. Again all curves have a steplike structure (non-Debye broadening) associated with polaron formation. The break point for each curve is again very close to the sample's Curie temperature.

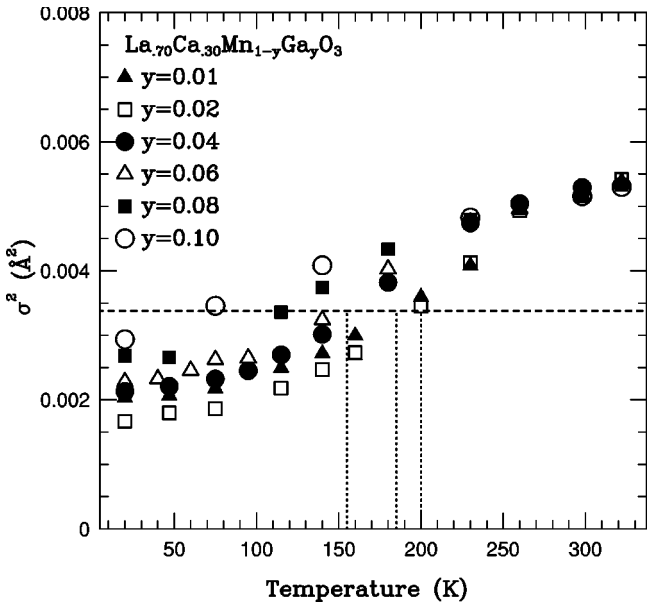

FIG. 14. A plot of σ^2 vs temperature for the Ga doped samples. Relative error bars are approximately the size of the symbols. The vertical dotted lines show the position of the peak in resistivity T_{MI} for $x=0.01$, 0.02, and 0.04 Ga doped samples. The horizontal line passes through the values of σ^2 at T_{MI} for each sample. This determines σ_c.

The inhomogeneous 0.01 sample does not follow this trend and is not included in our discussion but it is plotted as we show T_{MI}. The data at 300 K show that the relative change in static distortion with y is very small. The step in σ^2 below T_c again decreases with y, but the decrease is less than for the Ti doped samples (compare Fig. 14 with Fig. 13). The vertical dotted lines show the position of T_{MI} for the 1, 2 and 4% Ga doped samples, respectively. Again the dashed line corresponds to the points where the vertical lines cross each σ^2 vs T plot. Although we only have the resistivity peak temperatures for a few samples, these points again appear to give a constant value of σ_c^2. Note that σ_c^2 is higher than for the Ti doped samples, indicating that less distortion needs to be removed to produce the MI transition in the Ga doped samples.

In earlier studies we have shown that the decrease in σ^2 that occurs as T drops below T_c (associated with a decrease in the number of polarons), is an exponential function of the magnetization.[10] To compare the present data with previous results we first define this decrease $\Delta\sigma^2$ by the equation.

$$\Delta\sigma^2=\sigma_T^2+\sigma_{FP}^2+\sigma_{static}^2-\sigma_{Mn\text{-}O}^2, \tag{5}$$

where σ_T^2 is the thermal contribution calculated from $CaMnO_3$ (the solid line in Fig. 13) and $\sigma_{Mn\text{-}O}^2$ is the real data plotted in Figs. 13 and 14. The difference between $\sigma_T^2+\sigma_{static}^2$ and $\sigma_{Mn\text{-}O}^2$ at high temperature is called the full polaron distortion σ_{FP}^2 in Eq. (5).[9,10] σ_{static}^2 is the excess (above σ_T^2) contribution to σ^2 at 20 K.

Figure 15 shows a plot of $\ln\Delta\sigma^2$ vs M/M_0 for both Ti and Ga doped samples. There is a linear relationship between $\ln\Delta\sigma^2$ and the relative magnetization (above $M/M_0\sim0.3$),

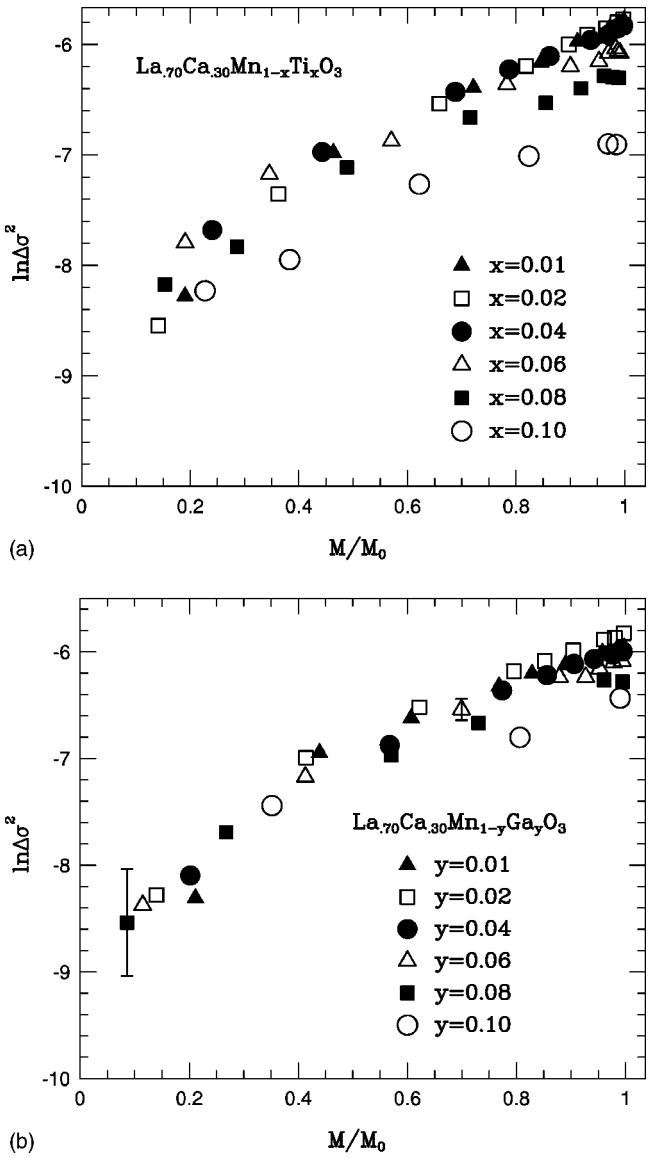

FIG. 15. Plots of $\ln\Delta\sigma^2$ vs M/M_0 for both the Ti and Ga doped samples. M is the measured magnetization and M_0 is the magnetization at the lowest temperature; M/M_0 is the relative magnetization. Representative error bars are shown in the lower panel at $M/M_0=0.086$ and 0.70. At high M/M_0, the error bars are smaller than the symbols.

which is consistent with our previous studies.[9,10] It provides evidence that there is a strong correlation between local structure and magnetism in these materials. As x,y increases, the slope of the straight line decreases slightly. There is some deviation from the straight line at low M/M_0. This may in part be caused by the much larger error in the data at lower magnetization, but is most likely related to the increased broadening of the transition and the long high-temperature tail above T_c (the magnetization is still not zero at 300 K).

From Figs. 1 and 2, we find that the resistivity peak for Ti occurs when the magnetization reaches a nearly constant value 16 000–18 000 emu/mole; the relative magnetization M/M_0, is very high for the Ti doped samples and varies from 0.75 to 0.95 for $x=0.01$ to 0.06. However, the plot of $\ln\Delta\sigma^2$

vs M/M_0 remains a straight line over this range. This is important evidence for a strong correlation between local structure and magnetization in CMR materials. The Ga doped samples show very similar results; the resistivity peak occurs when the magnetization reaches 13 500–14 000 emu/mole and the relative magnetization is near 65% for the few samples measured.

VI. ANALYSIS AND DISCUSSION

At the lowest temperatures the resistivity begins to increase for all the doped samples (around 5–20 K), suggesting an activated process. This behavior can be modeled by either variable range hopping between metallic clusters formed below T_c,[28] for which $\rho_{\mathrm{low}T}$ is given by

$$\rho_{\mathrm{low}T}=\rho_0\cdot e^{[E_b/(kT)]^{1/4}}, \tag{6}$$

or by a granular system model in which Coulomb effects are important.[29] In this case,

$$\rho_{\mathrm{low}T}=\rho_0\cdot e^{[E_b/(kT)]^{1/2}}. \tag{7}$$

Although the two equations differ in the temperature dependence of the exponent, the low temperature data can be fit equally well by either expression over the available temperature range, and we will only use the latter in the following discussion.

At high temperature, above T_c, previous work[30] has shown that the resistivity of a CMR material follows the activated adiabatic small polaron equation[23]

$$\rho_{\mathrm{polaron}}=A\cdot T\cdot e^{E_a/(kT)}, \tag{8}$$

where A is a constant proportional to the number of carriers and E_a is an activation energy. Our data fit this model well at high temperature, although again we have a limited temperature range.

In contrast, the resistivity in the cross-over region is much more difficult to model, because we do not know how the resistivity is distributed throughout the sample. In the high temperature regime the activation energy does not change much with concentration, while the prefactor A increases slightly. This suggests that the main effect of the Ti or Ga defects is to localize some of the charge carriers—i.e., some of the polarons—in regions where the local distortions are largest. In other regions, the average hopping rate is nearly unaffected. The fraction of localized carriers increases with Ti or Ga concentration.

Qualitatively a similar result is obtained from the changes in σ^2 in the XAFS data—there is an increase in the amount of static disorder in the sample with increasing x, which in turn would lead to an increased resistivity. However, the increase in static disorder only roughly tracks the increase in resistivity.

At low temperatures (but ignoring the lowest few data points for now) the resistivity changes by many orders of magnitude with x and y. This must be a combination of the size, shape, and increased resistivity of the FM regions as a result of the Ti or Ga doping, and possibly an increased resistivity of the nonmagnetic material at low T. Note that although a large fraction of the sample becomes magnetized at $x,y=0.1$ at low temperature, much of the sample remains distorted. Thus most of the magnetic sites must be partially distorted which would decreases the DE interaction. Since the conductivity is also very strongly dependent on the bond lengths, a slight increase in the local distortions within a cluster could explain both the large increase of the low temperature resistivity, and the low temperature required to achieve saturation of the magnetization. Because the resistivity does turn up at the lowest temperatures, some type of activation-like model is also needed at the very lowest temperatures.

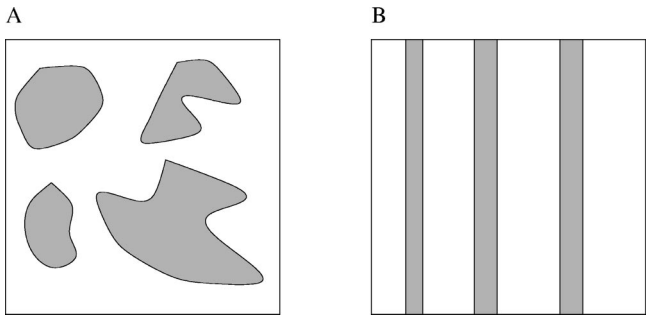

FIG. 16. Two different models describing the FM and non-FM regions in a CMR sample. Panel A: FM regions are shown as clusters; panle B: FM regions are shown as stripes. The dark region represents the FM region and the white region represents the non-FM region.

We have considered several models in attempting to model the crossover regime as some weighted average of the resistivity of the conducting regions and the high polaron-resistivity of the remaining material. We expect the fraction $z(T)$, of conducting material to increase as T decreases, crudely following the fraction of magnetized material $z(T)\sim M/M_0$. However the model will depend directly on the shape of the magnetic regions. Recently Moreo *et al.*[31] have considered different geometries for the FM regions—which can be classified as either stripes or clusters (see Fig. 16). A general stripe model would include long irregular FM filaments which may occasionally cross. Then the two resistivities would be combined in parallel and the resistivity would be similar to that for two-fluid models.[10,32] For this case, consider a slice of the sample to have a fraction $z(T)$, that is the conducting FM material ($\rho_{\mathrm{low}T}$) and the remainder $[1-z(T)]$ to have the polaron resistivity (ρ_{polaron}). The effective parallel resistivity is then given by

$$\rho_{\mathrm{effective}}=\frac{\rho_{\mathrm{polaron}}\cdot\rho_{\mathrm{low}T}}{\rho_{\mathrm{polaron}}\cdot z+\rho_{\mathrm{low}T}\cdot(1-z)}. \tag{9}$$

For low Ti or Ga concentrations, $z\sim 1$ at low T and becomes zero at high T. A simple function to model z is given by

$$z(T)=\frac{1}{1+e^{(T-T_F)/T_0}}, \tag{10}$$

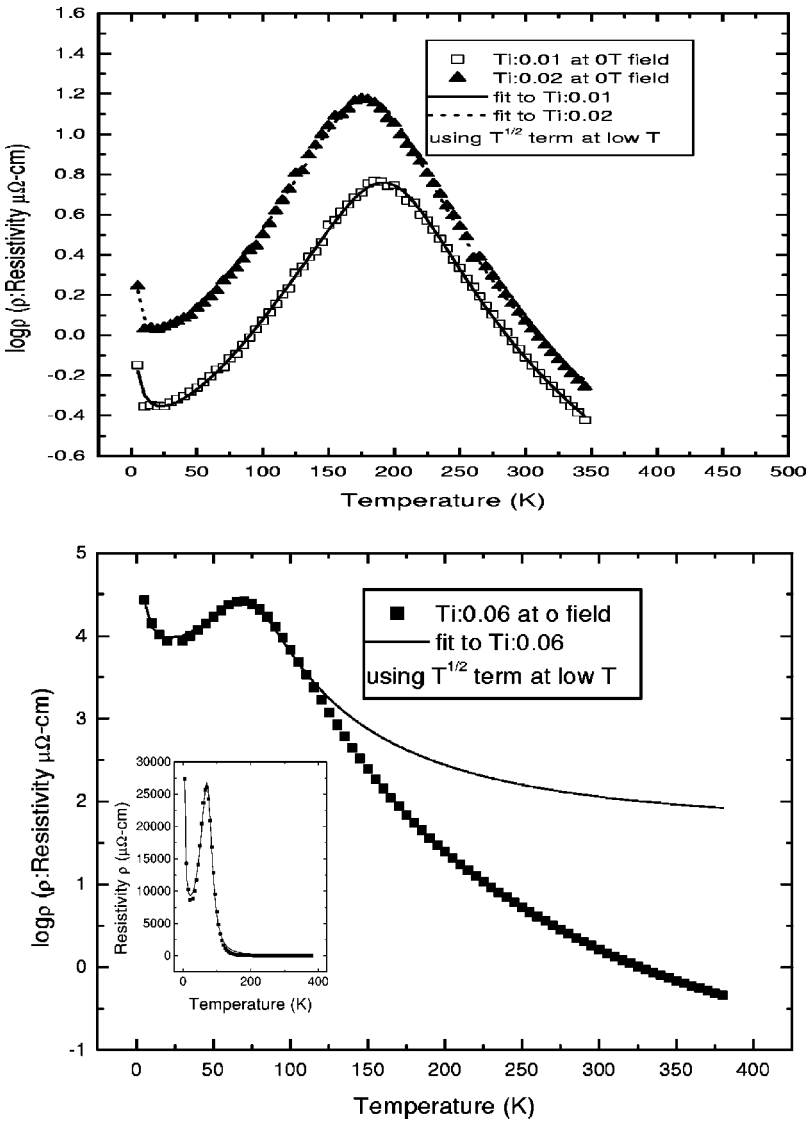

FIG. 17. Fits of the resistivity data for Ti:0.01, Ti:0.02, and Ti:0.06 samples at zero magnetic field, with the $T^{1/2}$ term in the exponent at low temperatures [Eq. (7)]. The top panel shows a good fit for the Ti:0.01 and Ti:0.02 samples, while the bottom panel shows a poor fit to the Ti:0.06 sample. The fit was carried out on a log scale. The inset in the bottom panel shows a fit to the Ti:0.06 sample on a linear scale; although it appears to be a good fit at this scale, the high temperature part does not fit well, as seen more clearly on the log scale.

where T_F determines the temperature at which $z=1/2$ and T_0 determines the temperature range over which the increase in z occurs.

We have fit the $x=0.01$, 0.02, and 0.06 data for the Ti doped sample to Eq. 9 using the appropriate functions in Eqs. (6)–(8) and (10). In Fig. 17 we show the fits on a log-linear plot using Eq. (7) for $\rho_{\mathrm{low}T}$. We can obtain a good fit for both low concentration samples, including the high magnetic field data (and using either Eq. (6) or (7) to describe the low T results); however, we cannot obtain a good fit in the crossover regime for any of the higher Ti or Ga concentrations. Moreover, even the fit for the low concentration sample does not make sense because the crossover function $z(T)$, required to achieve the fit remains essentially zero until $T<T_{\mathrm{MI}}$. It does not begin to increase until T is very low as shown in Fig. 18 where we compare the mixing functions from two other models with $z(T)$. The other two curves in Fig. 18 begin to increase when T is close to T_c. Although the ordered conducting FM regions have clearly formed (as evidenced by the drop in σ^2 for $x=0.01$) they do not become connected until T is well below T_c. Charge carriers may be able to hop relatively freely within these clusters, but transport between magnetic regions is inhibited until $T<T_{\mathrm{MI}}$.

This suggests that isolated magnetic clusters must form initially in this material as T is lowered below T_c (see Fig. 16). In this case, the highly resistive nonmagnetic material will dominate the resistivity until the regions between clusters becomes thin enough that they are no longer a barrier to conduction. However, applying such a model is not straight forward. First note that for a collection of uniform spherical clusters, the clusters would begin to touch when only 52% of the sample became magnetic. Experimentally a much higher magnetization must be achieved before the resistivity begins to fall. As a result a simple series combination of the resistivities also does not fit the data.

For the high concentration samples we have fit the high T range to obtain values of E_a and A–see Table III. We find that the activation energy for the adiabatic polaron resistivity E_a is almost independent of Ti concentration, as noted earlier, but is considerably larger than reported for other CMR systems.[30] We also find that E_a decreases slightly in a magnetic field.

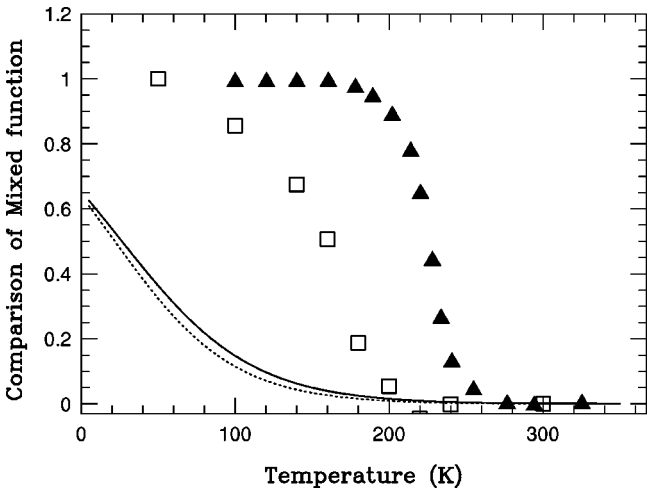

FIG. 18. A comparison between our mixing function $z(T)$ and mixing functions from other models. The solid line and the dotted line shows the $z(T)$ function for Ti:0.01 and Ti:0.02 samples, respectively. The solid triangle shows the mixing parameter c from a two-fluid model (Ref. 32) for 33% Ca doped LCMO sample. The open square shows the $\Delta\sigma^2$ function from our previous work (Ref. 10) for the 21% Ca doped LCMO sample, which we proposed to be proportional to the delocalized hole concentration n_{dh}.

Another interesting feature for the higher concentration samples is that the sample is still highly disordered even when the sample has become magnetic at low temperatures (see Figs. 13 and 14). For example, for the $x=0.08$ Ti doped sample, less than 50% of the local distortion is removed when T drops to 20 K, yet the saturated magnetization only drops about 14% (of which 6.5% is expected because of the nonmagnetic Ti). Within the DE model the Mn spins are coupled when the charge carriers can hop freely from one site to another at low temperatures. However, our data show that even when the sample is quite highly disordered at low temperature, it still can be almost fully ferromagnetic. There are several possible explanations for this behavior. (1) The DE mechanism can operate even when the electrons are hopping more slowly, such that the lattice has time to partially distort. (2) The net distortion about a Mn site is the sum of a static distortion (which increases with doping) plus a contribution from polarons. (3) There is some other mechanism than the DE mechanism for low temperature ferromagnetic ordering. However there is no compelling evidence for explanation (3) and we do not consider it further. The data can be explained as a combination of points (1) and (2) above. A static distortion of many sites would explain in part both the reduced amplitude of the Mn-O peak at low T and hence an increased value of σ^2 (see Fig. 11), and also the increased resistivity well above T_c. However, the more distorted sites would probably localize polarons and would likely be antiferromagnetic (AF), since in the absence of DE, $LaMnO_3$ is AF. The fraction of distorted sites must be considerably larger than the number of substituted sites.

We note that for these codoped samples, one cannot associate the magnitude of the local distortions observed at high temperatures, with only polaronlike distortions that are determined by the fraction of Mn in Mn^{3+} sites. From Table II as x increases, the fraction of Mn in Mn^{3+} sites increases for Ti doping and decreases for Ga doping. If no other static distortions existed, the polaron contribution to σ^2 should increases with x for Ti (a larger fraction of Mn is Mn^{3+}) and decrease for Ga. In contrast, there is a larger suppression of the polaron contribution for the Ti doped samples than for the Ga doped samples. Note that Ti is more effective in changing the average Mn valence of the sample than the Ga dopant and likely induces a larger local strain as a result in the increase in atomic radii; from these perspectives, the effects for Ti should be larger.

Finally other investigators have also carried out Mn site doping experiments but with different ions, including Co, Cr, and Fe. Toulemonde *et al.* show that for $Nd_{0.5}Ca_{0.5}Mn_{1-x}Co_xO_3$ and $Sm_{0.5}Ca_{0.5}Mn_{1-x}Cr_xO_3$ samples, the amplitude of the resistivity peak becomes smaller when the amount of Co increases. The resistivity peak temperature, T_{MI}, increases as x increases (except for the $x=0.06$ $Nd_{0.5}Ca_{0.5}Mn_{1-x}Co_xO_3$ sample),[33] which is quite different from the behavior discussed here.

VII. CONCLUSION

We have studied the effect of substitution on the Mn sites with nonmagnetic Ti^{+4} and Ga^{+3} ions in $La_{0.7}Ca_{0.3}MnO_3$. At

TABLE III. Fit results at high T [Eq. (8)] for the Ti and Ga doped samples. Here we have only fit to data well above T_{MI}.

Ti doped samples			Ga doped samples		
x	A	E_a/k	x	A	E_a/k
0.02; 0 T	$4.09(0.05)\times10^6$	2061(4)	0.02; 0 T	$4.59(0.07)\times10^6$	1659(6)
0.02; 6 T	$5.13(0.16)\times10^6$	1969(9)	0.02; 6 T	$6.01(0.03)\times10^6$	1547(2)
0.04; 0 T	$3.48(0.03)\times10^6$	2108(2)	0.04; 0 T	$2(0.1)\times10^5$	1632(23)
0.04; 6 T	$4.18(0.06)\times10^6$	2034(4)	0.04; 6 T	$2(0.1)\times10^5$	1602(16)
0.06; 0 T	$4.37(0.03)\times10^6$	2135(2)			
0.06; 6 T	$4.95(0.03)\times10^6$	2083(2)			
0.10; 0 T	$1(0.05)\times10^5$	2202(12)	0.10; 0 T	$1(0.06)\times10^5$	2177(16)
0.10; 6 T	$1(0.05)\times10^5$	2172(12)	0.10; 6 T	$1(0.07)\times10^5$	2146(18)

low Ti or Ga concentrations (x and y), the saturated magnetization decreases with increasing concentration, consistent with a reduction in the number of magnetic ions in the sample. However, for the high-concentration samples the effect is too large and cannot be explained by just the number of magnetic Mn sites removed. A possible interpretation is that the Ti^{+4} and Ga^{+3} ions generate small nonferromagnetic (paramagnetic or possibly antiferromagnetic) regions around them. T_c for these samples only shows a small concentration dependent effect, decreasing from 271 to 217 K for the Ti doped samples as x increases from 0.01 to 0.10 (although the transition is broadened); the Ga doped samples show a similar behavior.

The resistivity of these samples increases with Ti or Ga concentration, especially at low temperature, while T_{MI} shifts rapidly to lower temperatures as x,y increases. The increase of resistivity with x at high temperature suggests that some polarons are localized near the Ti defects (similar behavior for Ga). Although the magnetic and transport properties for the Ga doped samples are qualitatively similar to that for the Ti doped samples, the Ga^{3+} ion is found to be less effective in changing magnetization and resistivity of the sample than the Ti^{4+} ion.

A comparison between the magnetization and resistivity data for the codoped samples shows a very large difference between T_{MI} and T_c; in some cases T_{MI} can be up to 200 K below T_c. Such a large difference between T_c and T_{MI} suggests that these two transitions are not strongly correlated. A large MR is found for each of these samples; MR% increases dramatically with concentration, and can reach 1500% for the $x=0.06$ Ti doped sample. However, in contrast to the usual behavior for the manganite CMR systems, T_{MI} does not change very much with an applied external magnetic field.

A fit to the resistivity data was carried out for the Ti doped samples using a two-fluid model, where a parallel combination was applied to two types of conducting regions. The adiabatic polaron model was used for the high-temperature resistivity, while either a variable range hopping model or a granular system model was used to fit the low-temperature data. Although this model can fit the low concentration data well (Ti:0.01, 0.02), it does not fit the Ti:0.06 data at high temperature at all. Even for the low concentration samples, the crossover from a polaron conductivity at high T to a variable range hopping model at low T occurs at a temperature well below T_{MI} (and far below T_c). This suggests that the two-fluid model does not work for these codoped CMR systems. It may be due to the formation of isolated magnetic clusters surrounded by highly resistive nonferromagnetic regions. Such magnetic clusters would not contribute significantly to the transport until the nonferromagnetic regions between the clusters become thin enough to let electron hop or tunnel through the insulating region.

Strong correlations were again found between local structure (specifically changes in σ^2 for the Mn-O bond) and magnetization in these codoped CMR materials, as observed previously. The break point in the σ^2 vs temperature plot, below which σ^2 decreases more rapidly as polarons are removed, is very close to T_c. A surprising, and as yet unexplained behavior is that the resistivity peak occurs when σ^2 is reduced to some critical value $\sigma^2_{c\mathrm{Ti}}$ which is approximately the same for all Ti doped samples. The behavior for the Ga doped samples is similar but the corresponding critical value $\sigma^2_{c\mathrm{Ga}}$ is higher. Another unusual feature for the high concentrations is that the fraction of magnetized sample is high, even though the sample remains significantly disordered at low T. Thus there is ferromagnetic coupling even when the sample is quite disordered. The increase of ρ as T is decreased from T_c to T_{MI} while σ^2 decreases over the same T range (sample becomes more ordered), suggests that small clusters of FM material are forming, but do not become connected and hence do not contribute to transport until $T \leqslant T_{MI}$. Thus both a comparison of the magnetic and transport properties as well as attempts to model the resistivity arrive at the same conclusion—that nonconnected FM clusters must form first, long before the resistivity begins to decrease as the temperature is lowered below T_c.

ACKNOWLEDGMENTS

This work was supported in part by NSF Grant No. DMR9705117. The experiments were performed at SSRL, which is operated by the U.S. DOE, Division of Chemical Sciences, and by the NIH, Biomedical Resource Technology Program, Division of Research Resources.

[1] C. Zener, Phys. Rev. **82**, 403 (1951).
[2] P.W. Anderson and H. Hasegawa, Phys. Rev. **100**, 675 (1955).
[3] P.G. de Gennes, Phys. Rev. **118**, 141 (1960).
[4] A.J. Millis, P.B. Littlewood, and B.I. Shraiman, Phys. Rev. Lett. **74**, 5144 (1995).
[5] H. Röder, J. Zang, and A.R. Bishop, Phys. Rev. Lett. **76**, 1356 (1996).
[6] A.J. Millis, B.I. Shraiman, and R. Mueller, Phys. Rev. Lett. **77**, 175 (1996).
[7] A.J. Millis, Phys. Rev. B **53**, 8434 (1996).
[8] A.J. Millis, R. Mueller, and B.I. Shraiman, Phys. Rev. B **54**, 5405 (1996).
[9] C.H. Booth, F. Bridges, G.H. Kwei, J.M. Lawrence, A.L. Cornelius, and J.J. Neumeier, Phys. Rev. Lett. **80**, 853 (1998).
[10] C.H. Booth, F. Bridges, G.H. Kwei, J.M. Lawrence, A.L. Cornelius, and J.J. Neumeier, Phys. Rev. B **57**, 10 440 (1998).
[11] S.J.L. Billinge, R.G. DiFrancesco, G.H. Kwei, J.J. Neumeier, and J.D. Thompson, Phys. Rev. Lett. **77**, 715 (1996).
[12] D. Cao, F. Bridges, D.C. Worledge, C.H. Booth, and T. Geballe, Phys. Rev. B **61**, 11 373 (2000).
[13] D. Cao, F. Bridges, C.H. Booth, and J.J. Neumeier, Phys. Rev. B **62**, 8954 (2000).
[14] G. Subías, J. García, M.G. Proietti, and J. Blasco, Phys. Rev. B **56**, 8183 (1997).

[15] T.A. Tyson, J. Mustre de Leon, S.D. Conradson, A.R. Bishop, J.J. Neumeier, H. Röder, and J. Zang, Phys. Rev. B **53**, 13 985 (1996).
[16] R.D. Shannon, Acta Crystallogr., Sect. A: Cryst. Phys., Diffr., Theor. Gen. Crystallogr. **32**, 7519 (1976).
[17] G.G. Li, F. Bridges, and C.H. Booth, Phys. Rev. B **52**, 6332 (1995).
[18] F. Bridges, C.H. Booth, and G.G. Li, Physica B **208&209**, 121 (1995).
[19] S.I. Zabinsky, J.J. Rehr, A. Ankudinov, R.C. Albers, and M.J. Eller, Phys. Rev. B **52**, 2995 (1995).
[20] T. M. Hayes and J. B. Boyce, in *Solid State Physics*, edited by H. Ehrenreich, F. Seitz, and D. Turnbull (Academic, New York, 1982), Vol. 37, p. 173.
[21] B. K. Teo, *EXAFS: Basic Principles and Data Analysis* (Springer-Verlag, New York, 1986).
[22] J.J. Rehr, C.H. Booth, F. Bridges, and S.I. Zabinsky, Phys. Rev. B **49**, 12 347 (1994).
[23] D. Emin and T. Holstein, Ann. Phys. (N.Y.) **53**, 439 (1969).
[24] M. Croft, D. Sills, M. Greenblatt, C. Lee, S.-W. Cheong, K.V. Ramanujachary, and D. Tran, Phys. Rev. B **55**, 8726 (1997).
[25] F. Bridges, C.H. Booth, G.H. Kwei, J. Neumeier, and G.A. Sawatzky, Phys. Rev. B **61**, R9237 (2000).
[26] F. Bridges, C. H. Booth, M. Anderson, G. H. Kwei, J. J. Neumeier, J. Snyder, J. Mitchell, J. S. Gardner, and E. Brosha, Phys. Rev. B **63**, 214405 (2001).
[27] H. Woo, T.A. Tyson, M. Croft, S-W. Cheong, and J.C. Woicik, Phys. Rev. B **63**, 134412 (2001).
[28] N.F. Mott, J. Non-Cryst. Solids **1**, 1 (1968).
[29] P. Sheng, Philos. Mag. B **65**, 357 (1992).
[30] D.C. Worledge, L. Mieville, and T.H. Geballe, Phys. Rev. B **57**, 15 267 (1998).
[31] A. Moreo, S. Yunoki, and E. Dagotto, Science **283**, 2034 (1999).
[32] M. Jaime, P. Lin, S.H. Chun, M.B. Salamon, P. Dorsey, and M. Rubinstein, Phys. Rev. B **60**, 1028 (1999).
[33] O. Toulemonde, F. Studer, A. Barnabé, A. Maignan, C. Martin, and B. Raveau, Eur. Phys. J. B **4**, 159 (1998).